Forschungszentrum Karlsruhe
in der Helmholtz-Gemeinschaft

Wissenschaftliche Berichte
FZKA 6961

Stellar Neutron Capture Cross Sections of the Lu Isotopes

K. Wisshak, F. Voss, F. Käppeler, L. Kazakov
Institut für Kernphysik

Februar 2004

FORSCHUNGSZENTRUM KARLSRUHE
in der Helmholtz-Gemeinschaft
Wissenschaftliche Berichte
FZKA 6961

STELLAR NEUTRON CAPTURE CROSS SECTIONS OF THE Lu ISOTOPES

K. WISSHAK, F. VOSS, F. KÄPPELER, and L. KAZAKOV[1],

Institut für Kernphysik

[1]Institute for Physics and Power Engineering, Obninsk–Kaluga Region, Russia

Forschungszentrum Karlsruhe GmbH, Karlsruhe
2004

Impressum der Print-Ausgabe:

Als Manuskript gedruckt

Forschungszentrum Karlsruhe GmbH
Postfach 3640, 76021 Karlsruhe

Mitglied der Hermann von Helmholtz-Gemeinschaft
Deutscher Forschungszentren (HGF)

ISSN 0947-8620

ABSTRACT

The neutron capture cross sections of ^{175}Lu and ^{176}Lu have been measured in the energy range from 3 to 225 keV at the Karlsruhe 3.7 MV Van de Graaff accelerator. Neutrons were produced via the ^{7}Li$(p, n)^{7}$Be reaction by bombarding metallic Li targets with a pulsed proton beam and capture events were registered with the Karlsruhe 4π Barium Fluoride Detector. The cross sections were determined relative to the gold standard using isotopically enriched as well as natural lutetium oxide samples. Overall uncertainties of $\sim$1% could be achieved in the final results, which are about a factor of five more accurate than previous data. Maxwellian averaged neutron capture cross sections were calculated for thermal energies between kT = 8 keV and 100 keV. These values are systematically larger by $\sim$7% than reported in recent evaluations.

ZUSAMMENFASSUNG

DIE STELLAREN (n,γ) QUERSCHNITTE DER Lu ISOTOPE

Die Neutroneneinfangquerschnitte von ^{175}Lu und ^{176}Lu wurden am Karlsruher 3.7 MV Van de Graaff Beschleuniger im Energiebereich von 3 bis 225 keV gemessen. Neutronen wurden über die ^{7}Li$(p,n)^{7}$Be–Reaktion durch Beschuss metallischer Li–Targets mit einem gepulsten Protonenstrahl erzeugt, und Einfangereignisse mit dem Karlsruher 4π Barium Fluorid Detektor nachgewiesen. Die Messung wurde relativ zum Gold Standard–Querschnitt mittels angereicherter und natürlicher Lutetiumoxyd–Proben durchgeführt. Insgesamt wurden Unsicherheiten von $\sim$1% erreicht. Die Ergebnisse sind damit um ungefähr einen Faktor fünf genauer als die Resultate früherer Arbeiten. Aus diesen Daten wurden die stellaren Einfangquerschnitte für thermische Energien von $kT = 8$ keV bis 100 keV berechnet, die systematisch um $\sim$7% über den in neueren Evaluationen angegebenen Werten liegen.

Contents

1 INTRODUCTION

One of the prime topics in the original proposal for the construction of the Karlsruhe $4\pi BaF_2$ detector nearly 20 years ago was the verification of the σN-systematics [1], the genuine characteristics of nucleosynthesis in the slow neutron capture process (or s process for short). The validity of the s-process concept, which is related to the He-burning zones in Red Giant stars, implies that the product of the abundances N_s produced in the s-process and neutron capture cross section $< \sigma >$ averaged over the thermal stellar spectrum, is a smooth function of mass number. In mass regions between magic neutron numbers, this function is expected to exhibit even an almost constant dependence on mass number, a behavior that corresponds to reaction flow equilibrium. This *local* equilibrium can best be tested in the mass region of the rare earth elements (REE). Due to their close chemical similarity the relative abundances of the REE in the solar system are very accurately defined by analyses of a primitive type of meteorites, the so-called carbonaceous chondrites [2]. In fact, the abundances of the 14 REE are known with $\approx$1.7%, much better than those of all other elements, which are known with uncertainties of 5% to 10%.

The REE comprise 55 stable isotopes with 40 being situated on the reaction path of s-process nucleosynthesis. Among the remaining cases, seven stable isotopes can be ascribed exclusively to the r process and eight to the p process, which are both related to explosive nucleosynthesis in supernovae. With the present experiment, the stellar neutron capture cross sections of 29 of these 40 isotopes have been determined with the Karlsruhe $4\pi BaF_2$ detector, including seven of the eight s-only isotopes in this mass region. The $\approx$1% cross section uncertainty, that can be achieved with this technique matches with the $\approx$1.7% uncertainty of the REE abundances, thus providing the most crucial test of the σN-systematics.

Nine of the remaining 11 isotopes are accessible to the activation technique, which has been proven to yield similar uncertainties. Indeed, several of these cases have been measured recently by activation [3, 4, 5]. In conclusion, the only missing relevant measurements on REE with the $4\pi BaF_2$ detector are those on the erbium isotopes, where appropriate samples are yet to be found. All results for the isotopic neutron capture cross sections of the REE were considered in a recent update of evaluated stellar (n,γ) rates [6].

The s-process reaction path in the vicinity of lutetium is sketched in Fig. 1. Lutetium is the last REE followed by the element hafnium. Due to its long half life of $t_{1/2}$=36 Gyr and the fact that ^{176}Lu is of pure s-process origin since the r-process contributions to $A = 176$ are contained in the Yb isobar, this isotope was initially considered as a potential nuclear chronometer for the age of the s elements. However, it was found that the thermal photon bath at typical s-process temperatures is energetic enough for induced transitions from the long lived ground state to the short lived isomer ($t_{1/2}$ = 3.68 h), thus dramatically reducing the effective half life to a few hours. This effect changes the information contained in the ^{176}Lu/^{176}Hf pair from a potential chronometer into a sensitive s-process thermometer [7, 8, 9].

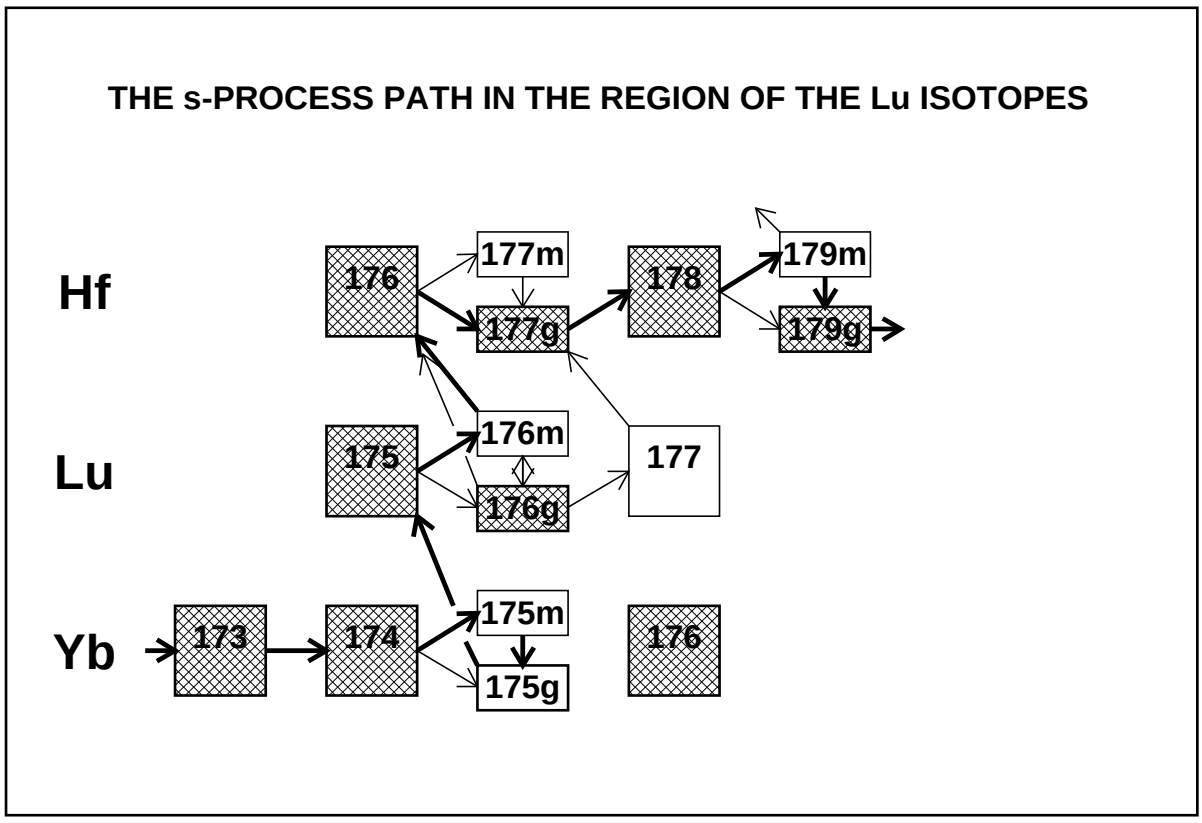

Figure 1: The reaction path of the s process in the region of the lutetium isotopes. Relevant isomeric states are indicated by separate boxes. Note that ^{176}Lu and ^{176}Hf represent s-only isotopes since they are shielded against β-decays from the r-process region by ^{176}Yb.

The present results together with the new data on the hafnium isotopes, recently completed in a parallel experiment [10], provide the basis for a refined analysis of the temperature sensitive branching at ^{176}Lu and a more reliable determination of the abundance of the s-only isotope ^{176}Hf. Another important input for this analysis is the solar Lu/Hf abundance ratio, which has been accurately determined by P.J. Patchett [11].

Due to its importance for s-process studies, lutetium has attracted considerable scientific interest. For ^{175}Lu a set of five time of flight (TOF) measurements of the neutron capture cross section in the relevant keV region are listed in the compilation of Bao *et al.* [6]. These experiments were facilitated by the natural ^{175}Lu abundance of 97.4% which does not require enriched sample material. The four measurements performed between 1972 and 1984 gave consistend results within the quoted uncertainties of 4% to 15%. The last measurement by Bokhovko *et al.* [12] from 1992, however, reported a much smaller cross section, which is incompatible with the previous data. For ^{176}Lu the low natural abundance requires enriched samples. These measurements were difficult since the available enrichment of only $\approx$72% implied considerable corrections for isotopic impurities. While the results of Beer *et al.* [11] obtained in experiments at two different accelerators

were consistent within the quoted uncertainties of ≈5%, these data differ significantly from earlier TOF results reported by Shorin *et al.* [13] and by Macklin and Gibbons [14] as well as from an activation measurement of Beer and Käppeler [15].

In the present experiment both, a natural as well as a highly enriched sample was used to measure the neutron capture cross section of ^{175}Lu. In case of the less enriched ^{176}Lu sample, the necessary correction of isotopic impurities could be performed with significantly improved accuracy, taking advantage of the good resolution in gamma-ray energy of the Karlsruhe 4π BaF_2 detector.

Measurements and data analysis are described in Secs. 2 and 3, followed by a discussion of the results and uncertainties in Secs. 4 and 5. The stellar cross sections are presented in Sec. 6. The astrophysical implications will be addressed in a forthcoming publication.

2 EXPERIMENT

The neutron capture cross sections of the two stable lutetium isotopes 175 and 176 have been measured in the energy range from 3 to 225 keV using gold as a standard. Since the experimental method has been published in detail [16, 17], only a general description is given here, complemented with the specific features of the present measurement.

Neutrons were produced via the ^{7}Li$(p,n)^7$Be reaction by bombarding metallic Li targets with the pulsed proton beam of the Karlsruhe 3.7 MV Van de Graaff accelerator. The neutron energy was determined by time of flight (TOF), the samples being located at a flight path of 79 cm. The relevant parameters of the accelerator were a pulse width of <1 ns, a repetition rate of 250 kHz, and an average beam current of 2.0 μA. In different runs, the proton energy was adjusted 30 and 100 keV above the threshold of the ^{7}Li$(p,n)^7$Be reaction at 1.881 MeV. In this way, continuous neutron spectra in the proper energy range for s–process studies were obtained, ranging from 3 to 100 keV, and 3 to 225 keV, respectively. The lower maximum neutron energy offers a significantly better signal-to-background ratio at lower energies.

Capture events were registered with the Karlsruhe 4π Barium Fluoride Detector via the prompt capture γ–ray cascades. This detector consists of 42 hexagonal and pentagonal crystals forming a spherical shell of BaF_2 with 10 cm inner radius and 15 cm thickness. It is characterized by a resolution in γ–ray energy of 7% at 2.5 MeV, a time resolution of 500 ps, and a peak efficiency of 90% at 1 MeV. The 1.7 MeV threshold in γ–ray energy used in the present experiment corresponds to an efficiency for capture events of more than 95% for all investigated isotopes. A comprehensive description of this detector can be found in Ref. [18].

The experiment was divided into three runs, two using the conventional data acquisition technique with the detector operated as a calorimeter, and one with an analog-to-digital converter (ADC) system coupled to the detector for analyzing the signals from all modules individually. In this way, the full spectroscopic information recorded by the detector can be recovered.

The lutetium samples were prepared from isotopically enriched oxide powder (Lu_2O_3) which was heated to 1200 K for 15 min to eliminate any water contaminations. Then the various batches were pulverized in an agate mortar, pressed into pellets 15 mm in

diameter and reheated to 1200 K for 1 h. During the final heating the pellets shrank slightly. Immediately after cooling, the actual samples were prepared by canning the pellets into air tight aluminum cylinders with 0.2 mm thick walls. Apart from the two lutetium samples, a gold sample in an identical can was used for measuring the neutron flux, and an empty can served for determining the sample-independent background. The background due to scattered neutrons was measured by means of a graphite sample. The relevant sample parameters and the isotopic composition of the lutetium samples are compiled in Tables 1 and 2. In the last run of the experiment the enriched ^{175}Lu sample was replaced by a sample made of natural lutetium oxide.

Table 1: SAMPLE CHARACTERISTICS

Sample	Diameter	Thickness		Weight	Can[b]	Neutron binding
	(mm)	(mm)	(10^{-3}at/barn)[a]	(g)	(g)	energy (MeV)
Graphite[c]	15.0	2.0	17.628	0.6213	0.187	
^{176}Lu	15.0	1.8	3.4139	2.0008	0.318	7.073
^{197}Au	15.0	0.4	2.2485	1.2996	0.258	6.513
^{175}Lu	14.6	0.9	1.1943	0.6974	0.244	6.293
Empty[c]	15.0				0.278	
^{nat}Lu[d]	14.4	1.3	1.7212	1.0052	0.251	

[a]For lutetium samples: sum of all Lu isotopes
[b]Aluminum cylinder
[c]Corresponding to sample order of runs I and II. In run III, the positions of the graphite sample and of the empty can were exchanged
[d]In run III, the natural lutetium sample was used instead of the enriched ^{175}Lu

Table 2: ISOTOPIC COMPOSITION (%)

Sample	Isotope	
	^{175}Lu	^{176}Lu
^{175}Lu	99.50	0.50
^{176}Lu	27.54	72.46
^{nat}Lu	97.41	2.59

The neutron transmission of the samples calculated with the SESH code [19] was generally larger than 95% (Table 3). The measured spectra of all samples were normalized to equal neutron flux by means of a ^{6}Li–glass monitor located close to the neutron target. The transmission spectra measured with a second ^{6}Li–glass detector at a flight path of 260 cm were used for a rough determination of the total cross sections. Though the accuracy of this method is inferior to that obtained in a dedicated experiment, these total cross sections can be used in the calculation of the multiple scattering correction.

The samples were moved cyclically into the measuring position by a computer controlled sample changer. The data acquisition time per sample was about 10 min, a complete cycle lasting about 0.8 h. From each event, a 64 bit word was recorded on DLT tape containing the sum energy and TOF information together with 42 bits identifying the contributing detector modules. The respective parameters of the three runs corresponding to neutron spectra with different maximum energies are listed in Table 4. The data in run III were recorded with the ADC system.

Table 3: CALCULATED NEUTRON TRANSMISSION[a]

Sample	Neutron Energy (keV)				
	10	20	40	80	160
^{197}Au	0.959	0.965	0.970	0.974	0.979
^{175}Lu	0.976	0.978	0.980	0.982	0.984
^{176}Lu	0.949	0.955	0.960	0.964	0.967
^{nat}Lu	0.966	0.970	0.973	0.975	0.977

[a] Monte Carlo calculation with SESH code [19].

Table 4: PARAMETERS OF THE INDIVIDUAL RUNS

Run	Flight Path (mm)	TOF Scale (ns/ch)	Number of Cycles	Maximum Neutron Energy (keV)	Measuring Time (d)	Mode of Operation	Average Beam Current (μA)	Threshold in Sum Energy (MeV)
I	788.5	0.7465	278	100	10.0	Calorimeter	1.8	1.7
II	788.5	0.7488	148	200	4.8	Calorimeter	2.0	1.7
III	786.6	0.6960	222	100	6.8	ADC	2.1	1.7

3 DATA ANALYSIS

3.1 Total Cross Sections

The total cross sections of the investigated isotopes were determined in the neutron energy range from 10 to 200 keV via the TOF spectra measured with the ^{6}Li glass detector at a flight path of 260 cm. The total cross sections and the related uncertainties were obtained as described in Ref. [16] and are listed in Table 5. The results deduced for the carbon sample agree with the data from the Joint Evaluated File (JEF) [20] in the energy range from 15 to 100 keV within $\pm 5.0\%$, except in the two energy bins from 30 keV to 40 keV and from 80 keV to 100 keV, where the aluminum of the sample cans exhibits strong scattering resonances at 34 and 87 keV. As can be seen from Table 1 the mass of the can for the graphite sample was significantly lower than that of all other cans. This leads to an overcompensation of the effect due to neutron scattering on the aluminum can of the graphite sample in the corresponding bins and, consequently to systematically underestimated total carbon cross sections.

The quoted uncertainties were obtained under the assumption that they are inversely proportional to the fraction of neutrons interacting in the sample, $A = 1 - T$, where T is the transmission. For the carbon sample this fraction is $A = 7.2\%$, the related uncertainty of 5.0% being estimated from the comparison with the JEF data. The graphite and gold samples had also been used in similar experiments on hafnium isotopes [10]. The results for the carbon cross section of both experiments agree to better than 0.3% and for the gold cross section to better than 0.7% which documents the good reproducibility of the method.

Unfortunately, in the energy range from 10 to 100 keV no other experimental data could be found in the literature. On the other hand the results for both lutetium isotopes agree within the quoted uncertainties very well with the two evaluated nuclear data files JEF-2.2 and ENDF-BVI, both indicating the observed low dependence on neutron energy.

Table 5: MEASURED TOTAL CROSS SECTIONS [a]

Neutron Energy	Total Cross Section (barn)			
(keV)	^{175}Lu	^{176}Lu	^{12}C	^{197}Au
10 – 15	10.3	13.1	3.99	13.1
15 – 20	11.5	12.7	4.16	13.6
20 – 30	12.3	12.5	4.47	13.7
30 – 40	10.3	11.8	3.71	11.9
40 – 60	10.2	11.6	4.39	12.1
60 – 80	10.6	12.7	4.32	11.3
80 – 100	10.3	10.2	3.82	10.6
100 – 150	10.7	8.7	3.94	8.3
150 – 200	11.5	8.6	3.87	7.4
Typical Uncertainty (%)	23.6	8.8	5.0	12.3

[a]Determined from the count rate of the ^{6}Li glass neutron monitor at 260 cm flight path

3.2 Capture Cross Sections

The analysis was carried out in the same way as described previously [16, 17]. All events were sorted into two–dimensional spectra containing 128 sum energy versus 2048 TOF channels according to different multiplicities (evaluation 1). In evaluation 2, this procedure was repeated by rejecting those events, where only neighboring detector modules contributed to the sum energy signal. With this option, background from the natural radioactivity of the BaF_2 crystals and from scattered neutrons can be reduced. For all samples, the resulting spectra were normalized to equal neutron flux using the count rate of the ^{6}Li glass monitor close to the neutron target. The corresponding normalization factors are below 0.5% for all runs. The treatment of the two-dimensional spectra from the data recorded with the ADC system is slightly more complicated and was performed as described in Ref. [16].

In the next step of data analysis, sample-independent backgrounds were removed by subtracting the spectra measured with the empty can. A remaining constant background was determined at very long flight times, where no time-correlated events are expected. The resulting two-dimensional spectra for events with multiplicity >2 measured in run III are shown for the two investigated isotopes in Fig. 2. Note that events with low sum energy and large TOF are suppressed by a preprocessing option of the ADC system.

At this point, the spectra contain only events correlated with the sample. The next correction to be made is for isotopic impurities (see Ref.[16] for details). The respective coefficients are compiled in Table 6. Fig. 3 shows the TOF spectra of both lutetium samples as measured in run I before subtraction of the background from isotopic impurities together with this background. In case of the ^{176}Lu sample the correction is about 20% of the measured effect while it is hardly visible for the ^{175}Lu sample due to the high enrichement.

As discussed in Ref. [21] the present method to correct for isotopic impurities holds exactly only if all samples are about equal in weight as only then second order effects due to neutron multiple scattering and self-absorption are properly accounted for. In the present experiment the largest correction is necessary for the ^{176}Lu sample due to the ^{175}Lu admixture of 27.5%. The weight of the two samples differs by a factor of 2.8. Calculating the correction directly from from the isotopic matrix may, therefore, lead to an overcompensation due to the smaller self-shielding effect in the thin ^{175}Lu sample. With the good energy resolution of the 4π BaF_2 this effect can be verified in the corrected sum-energy spectrum of ^{176}Lu where this effect would cause a dip at 6.29 MeV, the binding energy of ^{175}Lu. However, as shown in Fig. 4, this is not observed in the present case.

Following the correction for isotopic impurities, the background due to capture of sample scattered neutrons was removed from the spectra by means of the data measured with the scattering sample. The binding energy of both lutetium isotopes is low enough, that the correction can be normalized using the pronounced peak in the sum-energy spectra at 9.1 MeV due to capture in the odd barium isotopes ^{133}Ba and ^{135}Ba (see Fig. 2). After this last correction, the final spectra contain only the net capture events of the investigated isotopes (bottom spectra in Fig. 2). The corrections for capture of scattered neutrons are shown for all measured isotopes in Fig. 5, and the corresponding signal/background ratios are listed for different neutron energies in Table 7.

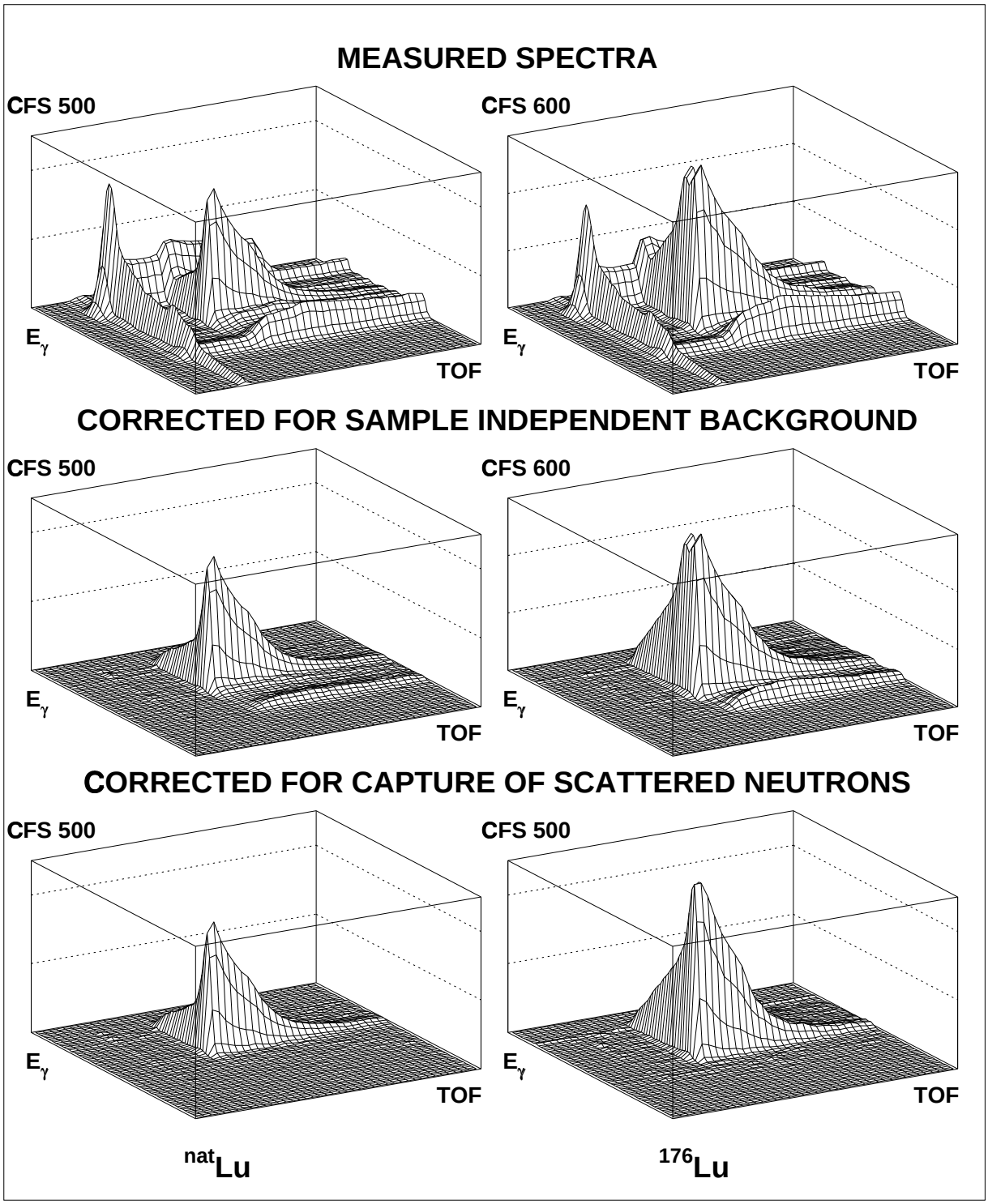

Figure 2: The different steps of background subtraction in the two–dimensional sum energy × TOF spectra. The data are shown for ^{nat}Lu and ^{176}Lu measured with the ADC system in run III with 100 keV maximum neutron energy. Only the events with multiplicity >2 are shown. (The original resolution of 128 × 2048 channels was compressed into 64 × 64 channels for better readability. Events at low sum-energy and large TOF are suppressed by the preprocessing in the ADC system.)

After subtraction of the scattering background the cross section shape versus neutron energy was determined from the TOF spectra of Fig. 5. These spectra are calculated by integrating the two-dimensional spectra in a region around the full energy peak. Due to the different background conditions in the spectra of events with different multiplicities, this range was chosen to decrease with multiplicity (see Fig. 7). For normalization, the two–dimensional data were projected onto the sum energy axis using the TOF region with optimum signal/background ratio as indicated in Fig. 5 by two vertical lines. The resulting pulse height spectra are shown in Fig. 6 for events with multiplicity >2. The threshold in sum energy is 1.7 MeV.

Table 6: MATRIX FOR ISOTOPIC CORRECTIONS (%)

Corrected spectrum	Measured spectrum		Corrected sample thickness
runs I, II	^{175}Lu	^{176}Lu	(10^{-3} at/barn)
^{175}Lu	100	–0.241	1.1860
^{176}Lu	–79.121	100	2.4690
run III	^{nat}Lu	^{176}Lu	
^{nat}Lu	100	–1.802	1.6597
^{176}Lu	–56.076	100	2.4487

Table 7: SIGNAL/BACKGROUND RATIO FOR RUNS WITH DIFFERENT MAXIMUM NEUTRON ENERGY

Sample	σ_t/σ_γ	Maximum neutron energy	Signal/Background ratio[a]		
	E_n=30 keV	(keV)	E_n=30 keV	E_n=20 keV	E_n=10 keV
^{175}Lu	10	100	15.3	7.3	4.0
^{176}Lu	8		11.3	6.0	4.0
^{197}Au	24		8.2	3.7	2.6
^{175}Lu		200	12.7	6.3	3.5
^{176}Lu			10.5	5.5	3.5
^{197}Au			7.0	3.6	2.3

[a]Defined as (effect+neutron scattering background)/(neutron scattering background)

The sum energy spectra of all isotopes are shown in Fig. 7 for different multiplicities. These multiplicities correspond to the number of detector modules contributing per event, which are slightly larger than the true multiplicities because of cross talking. The arrows in Fig. 7 indicate the range of sum energy channels that were integrated to obtain the TOF spectra of Fig. 5 for determining the cross section shapes.

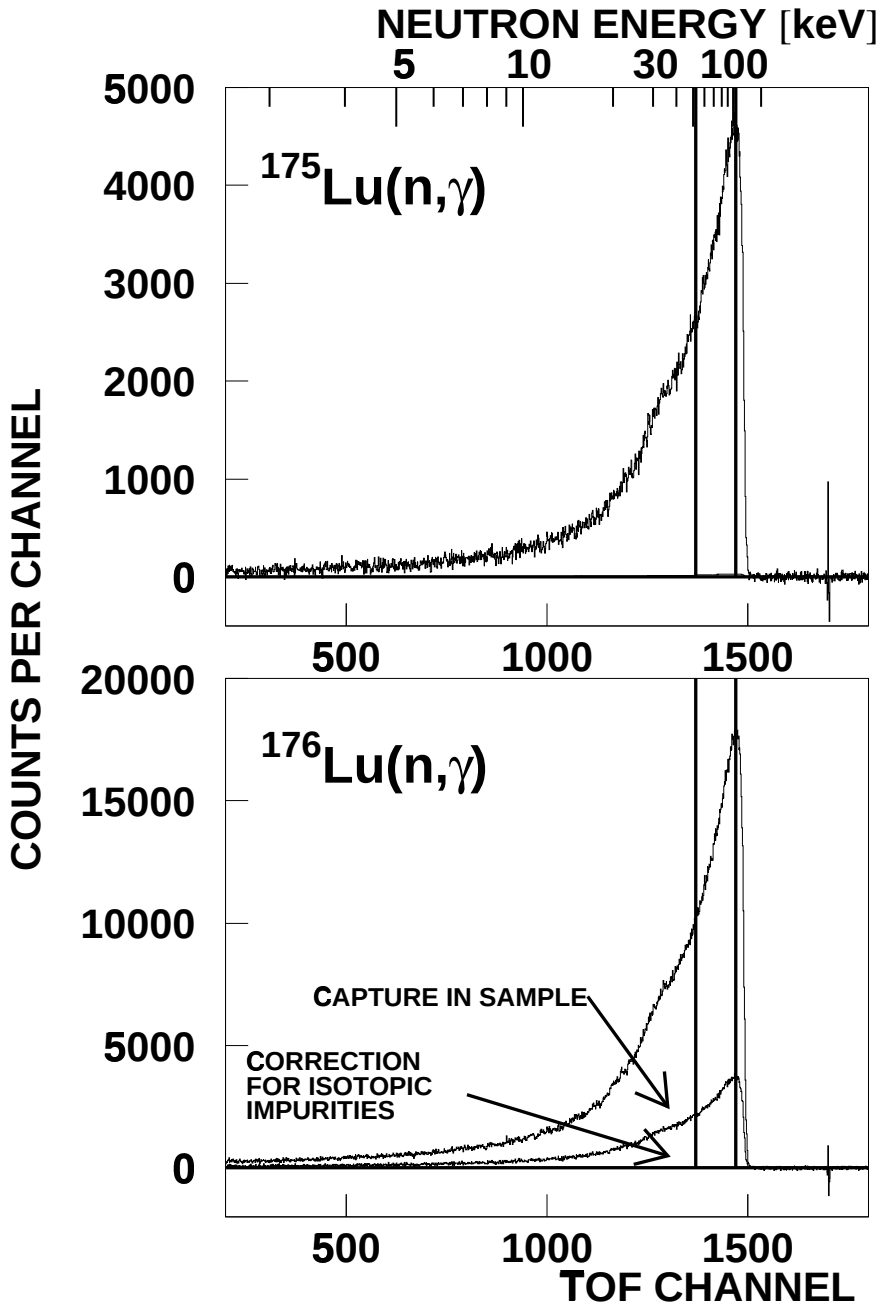

Figure 3: TOF spectrum of the lutetium samples measured in run I. The background due to isotopic impurities is shown separately. Due to the high enrichment of 99.5% it is hardly visible for the ^{175}Lu sample.

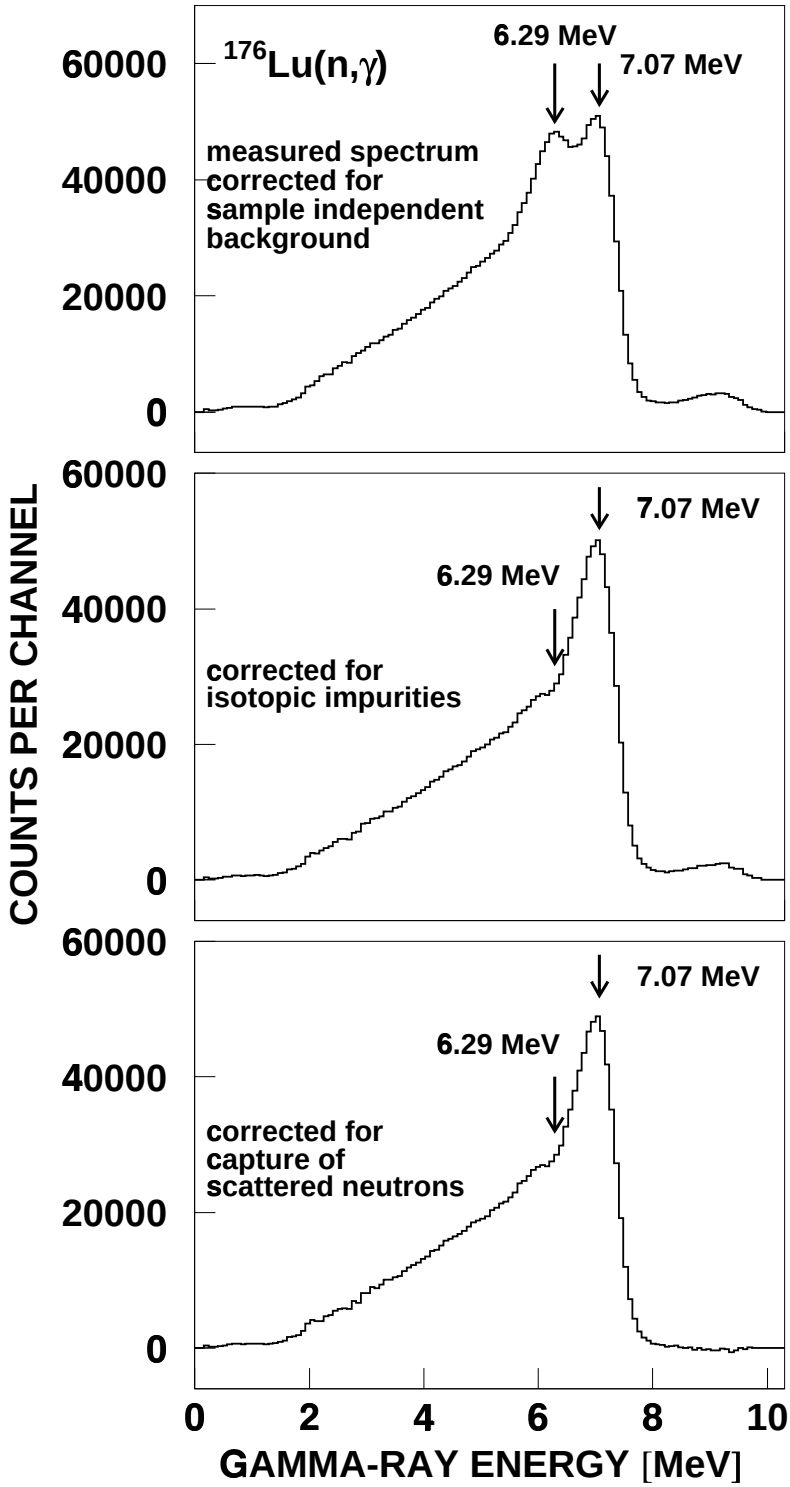

Figure 4: Sum-energy spectra of the ^{176}Lu sample. The correction of isotopic impurities according to the matrix given in Table 6 does not result in a dip at the position of the binding energy of ^{175}Lu (6.29 MeV), indicating an overcompensation as observed for a ^{176}Hf sample of compatibly low enrichment [10].

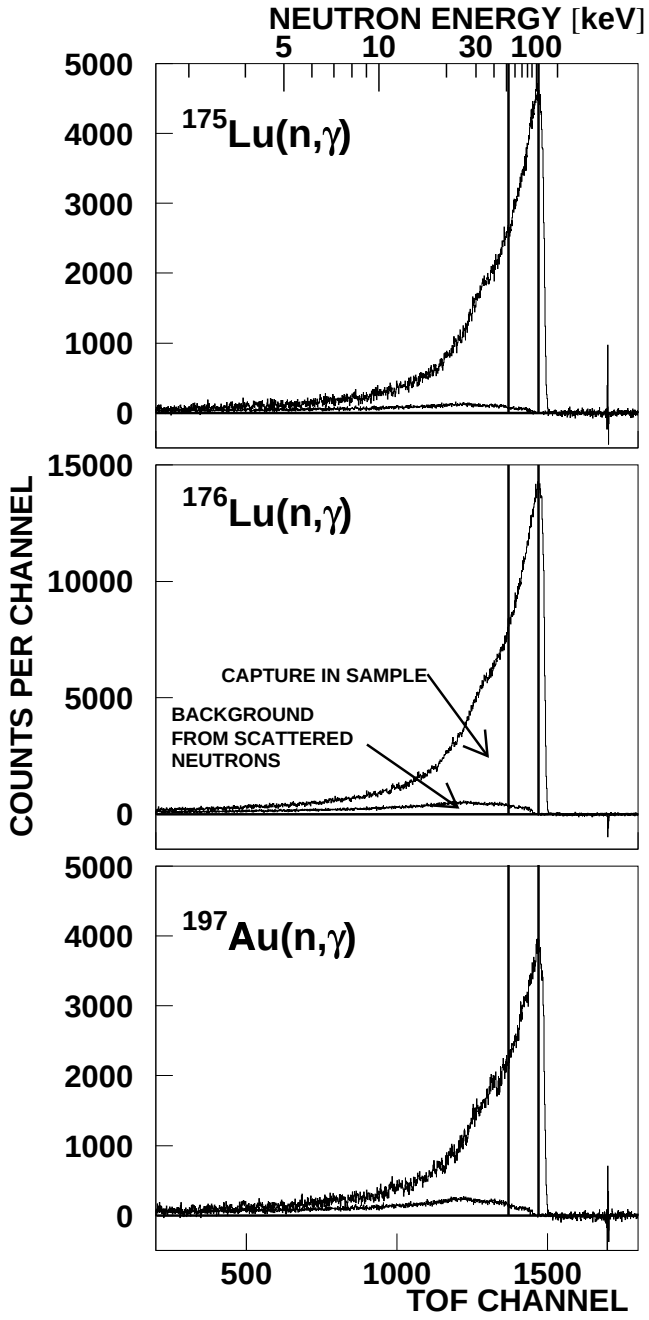

Figure 5: TOF spectra measured with all samples in run I (100 keV maximum neutron energy). The background due to sample scattered neutrons is shown separately. The region used for absolute normalization of the cross section is indicated by two vertical lines.

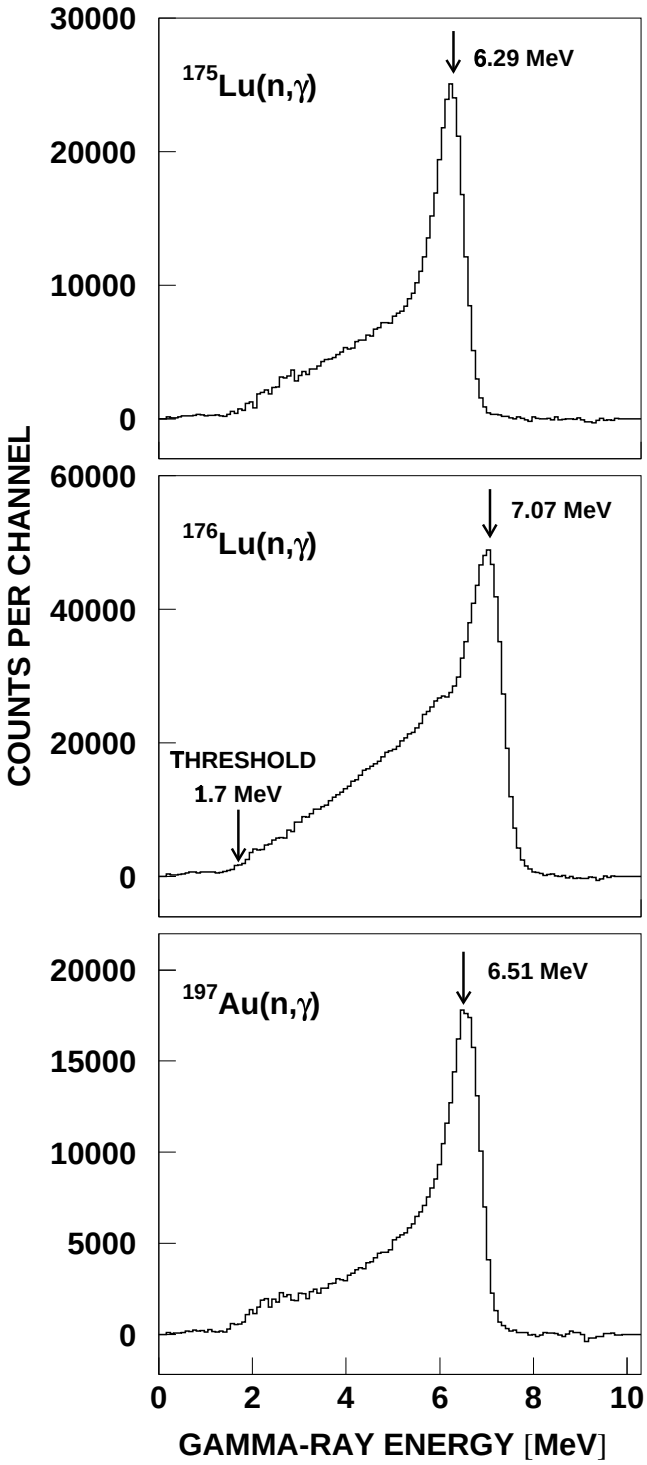

Figure 6: Sum energy spectra of all isotopes measured in run I containing events with multiplicity >2. These spectra were obtained by projection of the two–dimensional spectra in the TOF region below the maximum neutron energy as indicated by vertical lines in Fig. 5.

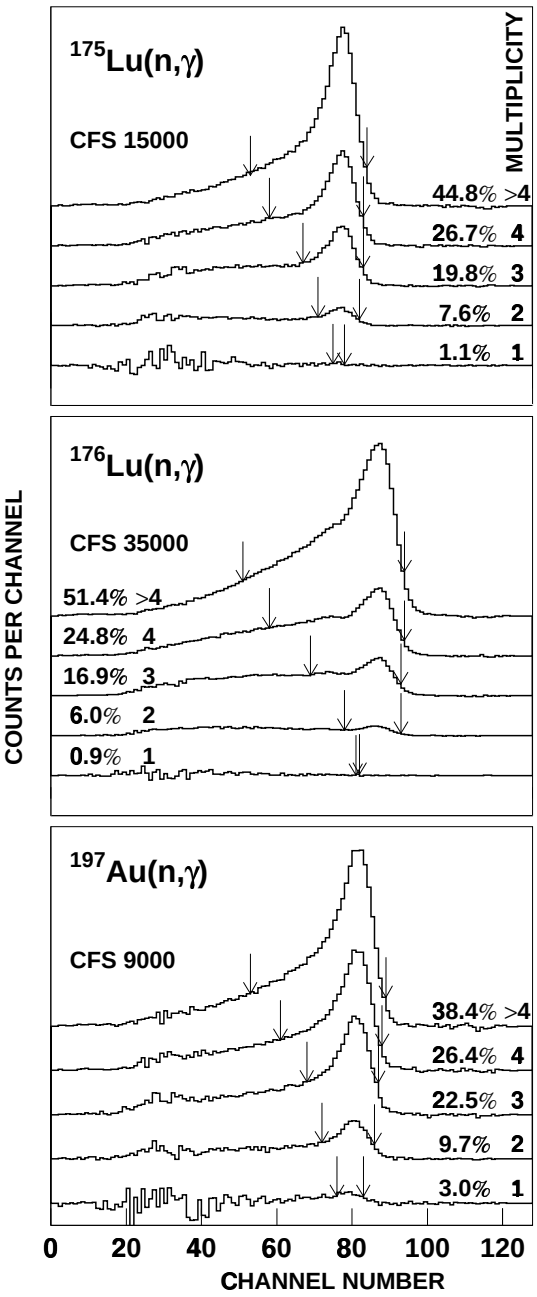

Figure 7: Sum energy spectra of all isotopes as a function of multiplicity. The regions integrated to determine the cross section shape (see TOF spectra of Fig. 5) are indicated by arrows.

The cross section ratio of isotope X relative to the gold standard is given by

$$\frac{\sigma_i(X)}{\sigma_i(Au)} = \frac{Z_i(X)}{Z_i(Au)} \frac{\Sigma Z(Au)}{\Sigma Z(X)} \frac{\Sigma E(X)}{\Sigma E(Au)} \frac{m(Au)}{m(X)} F_1 F_2. \quad (1)$$

In this expression, Z_i is the count rate of channel i in the TOF spectrum, ΣZ is the TOF rate integrated over the interval used for normalization (vertical lines in Fig. 5), ΣE is the total count rate in the sum energy spectra for all multiplicities in this TOF interval. The respective sum energy spectra are shown in Fig. 7. For all multiplicities these spectra were integrated from the threshold at 1.7 MeV beyond the binding energy, and the sum of these results, ΣE is used in Eq. 1. A full description of this procedure is given in Ref.[22]. The quantity m is the sample thickness in atoms/b. The factor $F_1 = [100 - f(Au)]/[100 - f(X)]$ corrects for the fraction of capture events f below the experimental threshold in sum energy, where X refers to the respective lutetium sample (Table 8), and F_2 is the ratio of the multiple scattering and self–shielding corrections.

The fraction of unobserved capture events, f, and the correction factor F_1 were calculated as described in Ref. [23]. The input for this calculation are the individual neutron capture cascades and their relative contributions to the total capture cross section as well as the detector efficiency for monoenergetic γ-rays in the energy range up to 10 MeV. As in the experiment on dysprosium isotopes [24] this information was derived directly from the experimental data recorded with the ADC system in run III. From these data, only events close to the sum energy peak (see Fig. 6) were selected, which contained the full capture γ-ray cascade. This ensemble was further reduced by restricting the analysis to the TOF region with optimum signal-to-background ratio (vertical lines in Fig. 5). The correction factors F_1 are quoted in Table 8.

The capture γ-ray spectra obtained from the data taken with the ADC system are shown in Fig. 8 in energy bins of 500 keV. The spectra of the two lutetium isotopes are fairly similar and significantly softer than the spectrum of the gold sample.

The correction for neutron multiple scattering and self-shielding was calculated with the SESH code [19]. Apart from the pairing energies [25], most of the input parameters were taken from Ref. [26], but were slightly modified in order to reproduce the measured total and capture cross sections. For the ^{175}Lu sample it was difficult to find adequate parameters that reproduce the experimentally observed flat shape of the cross section (see Table 5). The final values are listed in Table 9 together with the calculated total cross sections. The resulting correction factors, MS(X) and F_2, are compiled in Tables 10 and 11. In general, these corrections are smaller than 2%.

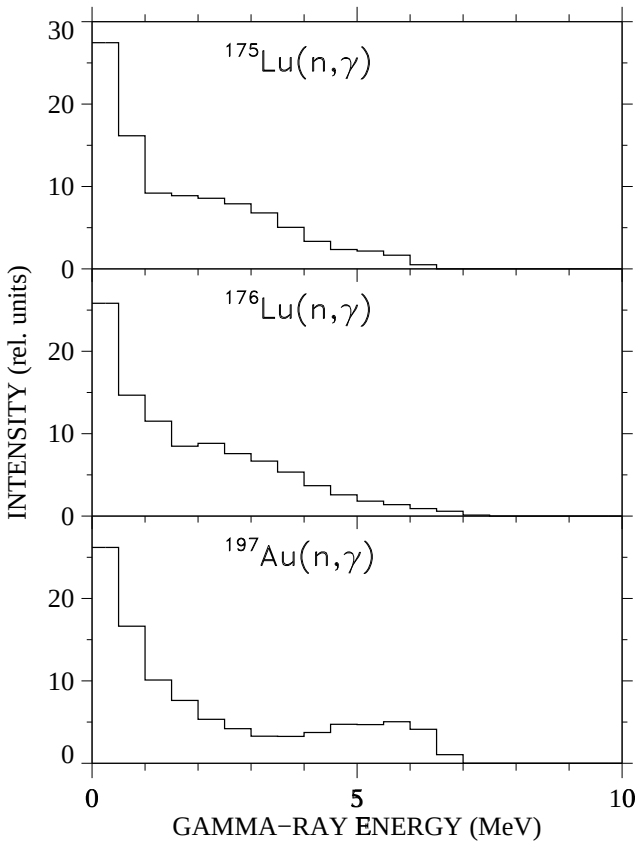

Figure 8: Capture γ-ray spectra derived from the capture cascades recorded with the ADC system. (The full resolution of 2048 channels is compressed into bins of 500 keV.)

Table 8: FRACTION OF UNDETECTED CAPTURE EVENTS, f (%), AND THE RELATED CORRECTION FACTORS F_1.[a]

	Threshold in Sum Energy (MeV)		
	1.5	1.7	2.0
f(Au)	5.15		7.09
f(^{175}Lu)	3.06		4.65
f(^{176}Lu)	1.99		3.15
F_1(^{175}Lu/Au)	0.978	0.977	0.974
F_1(^{176}Lu/Au)	0.968	0.964	0.959

[a] derived from capture cascades measured with the ADC system.

Table 9: PARAMETERS FOR THE CALCULATION OF NEUTRON SELF–SHIELDING AND MULTIPLE SCATTERING CORRECTIONS

Parameter		^{175}Lu	^{176}Lu	^{16}O
Nucleon Number		175	176	16
Binding Energy (MeV)		6.293	7.073	4.144
Pairing Energy (MeV)		0.0	0.400	0.0
Effective Temperature (K)		293	293	293
Nuclear Spin		3.5	7.0	0
Average Radiation	s	0.081	0.090	0
Width (eV)	p	0.028	0.022	
	d	0.018	0.012	
Average Level	s	3.45	1.74	0
Spacing (eV)	p[a]	1.73	0.87	
	d[a]	1.15	0.58	
Strength Function	S_0	1.8	2.0	0
(10^{-4})	S_1	0.8	1.0	
	S_2	3.0	3.0	
Nuclear Radius	s	8.0	7.7	5.5
(fm)	p	7.8	7.5	
	d	8.0	7.7	
	Calculated total cross sections			
3 keV		21.7	22.5	3.80
5 keV		18.5	19.0	3.80
10 keV		15.3	15.5	3.79
20 keV		13.0	13.0	3.77
40 keV		11.2	11.1	3.74
80 keV		9.7	9.6	3.68
160 keV		8.5	8.4	3.55
320 keV		7.5	7.6	3.31

[a]Calculated with SESH [19]

Table 10: CORRECTION FACTORS FOR NEUTRON SELF–SHIELDING AND MULTIPLE SCATTERING, MS

Energy Bin	MS			
(keV)	^{197}Au	^{175}Lu	^{176}Lu	^{nat}Lu
3 – 5	0.994	1.015	1.015	1.012
5 – 7.5	1.016	1.017	1.020	1.017
7.5 – 10	1.028	1.018	1.022	1.019
10 – 12.5	1.033	1.019	1.023	1.020
12.5 –15	1.036	1.019	1.023	1.020

Table 10 (continued)

15 – 20	1.038	1.019	1.023	1.020
20 – 25	1.038	1.019	1.023	1.020
25 – 30	1.038	1.018	1.023	1.020
30 – 40	1.037	1.018	1.023	1.019
40 – 50	1.036	1.018	1.023	1.019
50 – 60	1.035	1.018	1.023	1.019
60 – 80	1.034	1.017	1.022	1.019
80 – 100	1.032	1.017	1.022	1.018
100 – 120	1.031	1.017	1.022	1.018
120 – 150	1.030	1.016	1.022	1.017
150 – 175	1.029	1.016	1.021	1.017
175 – 200	1.028	1.016	1.021	1.017
200 – 225	1.027	1.015	1.021	1.016
Uncertainty (%)	0.3	0.2	0.1	0.2

Table 11: CORRECTION FACTORS FOR THE CROSS SECTION RATIOS, F_2 = MS(Au)/MS(X)

Energy Bin	F_2		
(keV)	^{175}Lu/Au	^{176}Lu/Au	^{nat}Lu/Au
3 – 5	0.979	0.979	0.982
5 – 7.5	0.999	0.996	0.999
7.5– 10	1.010	1.006	1.009
10 – 12.5	1.014	1.010	1.013
12.5 – 15	1.017	1.013	1.016
15 – 20	1.019	1.015	1.018
20 – 25	1.019	1.015	1.018
25 – 30	1.020	1.015	1.018
30 – 40	1.019	1.014	1.018
40 – 50	1.018	1.013	1.017
50 – 60	1.017	1.012	1.016
60 – 80	1.017	1.012	1.015
80 – 100	1.015	1.010	1.014
100 – 120	1.014	1.009	1.013
120 – 150	1.014	1.008	1.013
150 – 175	1.013	1.008	1.012
175 – 200	1.012	1.007	1.011
200 – 225	1.012	1.006	1.011
Uncertainty (%)	0.4	0.3	0.4

4 DIFFERENTIAL NEUTRON CAPTURE CROSS SECTIONS

The measured neutron capture cross section ratios of the investigated Lu isotopes and of ^{197}Au are listed in Tables 12 and 13 together with the respective statistical uncertainties. The data are given for all runs and for the two evaluation methods discussed in Sec. 3. The last column in each table contains the weighted average, the weight being determined by the inverse of the squared statistical uncertainties. Since the cross section ratios depend weakly on energy, the averages for the energy interval from 30 to 80 keV are also included for a better comparison of the individual results. The data are free of systematic differences with respect to the various runs and evaluations and well consistent within the quoted statistical uncertainties. This holds also for the ^{175}Lu results, which were obtained with enriched and natural samples.

As in previous studies with the 4π BaF_2 detector [16, 17, 27], the final cross section ratios were adopted from evaluation 2. The respective mean values are compiled in Table 14 together with the statistical, systematic, and total uncertainties. The energy bins are sufficiently fine to avoid systematic effects in calculating the Maxwellian averaged cross sections (Sec. 6). In the energy bins from 15 to 200 keV statistical uncertainties below 1.0% could be obtained for all investigated cross sections. The systematic uncertainties range between 0.7 and 0.8%.

The experimental ratios were converted into absolute cross sections using the gold data of Macklin [28] after normalization by a factor of 0.989 to the absolute value of Ratynski and Käppeler [29] (Table 15). The uncertainties of the resulting values can be obtained by adding the 1.5% uncertainty of the reference cross section to the uncertainties of the respective cross section ratios.

The present results are compared in Fig. 9 to previous data of Beer *et al.* [11], Bokhovko *et al.* [12], and Macklin and Gibbons [14]. The 5 - 8% uncertainties of the older values could be significantly improved. While there is reasonable agreement with the data of Beer *et al.* [11], systematic differences are found with respect to the other two experiments.

Table 12: $\sigma(^{175}\mathrm{Lu})/\sigma(^{197}\mathrm{Au})$ AND STATISTICAL UNCERTAINTIES (in %)

Energy Bin (keV)	Run I		Run II		Run III		Average	
evaluation 1								
3 – 5	1.8238	9.0	1.6538	11.	1.7015	9.7	1.7359	5.6
5 – 7.5	1.8160	5.1	1.7124	7.1	1.6744	6.2	1.7483	3.4
7.5 – 10	2.0979	4.1	2.1305	6.0	1.9390	5.0	2.0549	2.8
10 – 12.5	1.8435	3.1	1.7213	4.6	1.8011	3.3	1.8039	2.0
12.5 – 15	2.1016	2.8	1.9669	3.8	1.9797	2.9	2.0260	1.8
15 – 20	2.1145	1.8	2.0387	2.4	2.1000	1.8	2.0924	1.1
20 – 25	2.2635	1.5	2.2124	2.0	2.3029	1.5	2.2671	0.9
25 – 30	2.2069	1.3	2.1227	1.6	2.1750	1.2	2.1743	0.8
30 – 40	2.1832	1.0	2.1340	1.1	2.1709	1.0	2.1655	0.6
40 – 50	2.2723	1.0	2.2631	1.2	2.2704	1.0	2.2692	0.6
50 – 60	2.2637	0.9	2.1842	1.2	2.2634	1.0	2.2435	0.6
60 – 80	2.2170	0.8	2.2235	0.9	2.2517	0.8	2.2308	0.5
80 – 100	2.2977	0.8	2.2899	0.9	2.3058	0.8	2.2983	0.5
100 – 120	2.1981	0.9	2.2548	0.9	2.2334	0.9	2.2268	0.5
120 – 150	–	–	2.0634	0.9	–	–	2.0634	0.9
150 – 175	–	–	1.9582	1.0	–	–	1.9582	1.0
175 – 200	–	–	1.9245	1.0	–	–	1.9245	1.0
200 – 225	–	–	1.8880	1.5	–	–	1.8880	1.5
30 – 80	2.2341	0.7	2.2012	0.6	2.2391	0.7	2.2273	0.4
evaluation 2								
3 – 5	2.1680	6.7	1.5535	9.1	1.7083	6.7	1.8569	4.3
5 – 7.5	1.8280	3.8	1.6527	5.5	1.7113	4.5	1.7513	2.6
7.5 – 10	2.1069	3.1	2.0292	4.7	1.9430	3.6	2.0354	2.1
10 – 12.5	1.8897	2.4	1.8358	3.4	1.8345	2.5	1.8575	1.6
12.5 – 15	2.0847	2.2	2.0180	3.1	1.9973	2.2	2.0356	1.4
15 – 20	2.1943	1.5	2.1174	1.9	2.1216	1.4	2.1478	0.9
20 – 25	2.2820	1.3	2.2600	1.6	2.2725	1.2	2.2732	0.8
25 – 30	2.2014	1.1	2.1315	1.3	2.1262	1.0	2.1538	0.6
30 – 40	2.1830	0.8	2.1507	0.9	2.1370	0.7	2.1558	0.5
40 – 50	2.2773	0.8	2.2667	1.0	2.2292	0.8	2.2551	0.5
50 – 60	2.2501	0.8	2.1829	1.0	2.2236	0.8	2.2234	0.5
60 – 80	2.2111	0.7	2.2124	0.8	2.2078	0.6	2.2101	0.4
80 – 100	2.2780	0.7	2.2831	0.8	2.2611	0.7	2.2728	0.4
100 – 120	2.1722	0.8	2.2383	0.8	2.1727	0.7	2.1917	0.4
120 – 150	–	–	2.0394	0.8	–	–	2.0394	0.8
150 – 175	–	–	1.9435	0.8	–	–	1.9435	0.8
175 – 200	–	–	1.8961	0.9	–	–	1.8961	0.9
200 – 225	–	–	1.8699	1.3	–	–	1.8699	1.3
30 – 80	2.2304	0.5	2.2032	0.5	2.1994	0.5	2.2111	0.3

Table 13: $\sigma(^{176}\mathrm{Lu})/\sigma(^{197}\mathrm{Au})$ AND STATISTICAL UNCERTAINTIES (in %)

Energy Bin (keV)	Run I		Run II		Run III		Average	
evaluation 1								
3 – 5	3.0579	7.7	1.6242	9.2	2.2113	8.9	2.3895	5.1
5 – 7.5	2.6606	4.3	2.1504	5.9	2.3027	5.6	2.4339	3.0
7.5 – 10	3.0128	3.6	2.8823	5.4	2.6562	4.7	2.8793	2.5
10 – 12.5	2.5793	2.7	2.3888	3.8	2.3754	3.1	2.4702	1.8
12.5 – 15	2.8991	2.5	2.5535	3.3	2.7421	2.8	2.7617	1.6
15 – 20	2.8919	1.6	2.6848	2.1	2.7495	1.7	2.7939	1.0
20 – 25	3.0608	1.4	2.9883	1.8	3.0591	1.4	3.0428	0.9
25 – 30	2.9538	1.1	2.8438	1.4	2.9211	1.2	2.9143	0.7
30 – 40	2.8677	0.9	2.8268	1.0	2.8952	0.9	2.8653	0.5
40 – 50	2.9532	0.9	2.9257	1.0	2.9573	0.9	2.9470	0.5
50 – 60	2.9938	0.8	2.9125	1.0	3.0229	0.9	2.9814	0.5
60 – 80	2.9577	0.7	2.9620	0.8	2.9973	0.8	2.9712	0.4
80 – 100	3.0275	0.7	3.0075	0.8	3.0588	0.8	3.0309	0.4
100 – 120	3.0100	0.8	3.0083	0.8	3.0274	0.9	3.0145	0.5
120 – 150	–	–	3.0433	0.7	–	–	3.0433	0.7
150 – 175	–	–	3.0542	0.8	–	–	3.0542	0.8
175 – 200	–	–	3.0038	0.9	–	–	3.0038	0.9
200 – 225	–	–	2.9153	1.2	–	–	2.9153	1.2
30 – 80	2.9431	0.6	2.9068	0.5	2.9682	0.7	2.9412	0.3
evaluation 2								
3 – 5	2.9677	6.1	2.0016	7.5	2.2035	6.4	2.4463	3.9
5 – 7.5	2.5967	3.3	2.1828	4.6	2.3482	4.2	2.4264	2.3
7.5 – 10	2.8669	2.8	2.9299	4.2	2.6286	3.4	2.8057	1.9
10 – 12.5	2.5933	2.1	2.4202	3.0	2.4574	2.4	2.5093	1.4
12.5 – 15	2.8938	2.0	2.6781	2.7	2.6933	2.1	2.7729	1.3
15 – 20	2.9675	1.3	2.7387	1.7	2.8099	1.4	2.8571	0.8
20 – 25	3.0634	1.1	3.1116	1.5	3.0288	1.1	3.0611	0.7
25 – 30	2.9532	0.9	2.9133	1.2	2.8856	0.9	2.9176	0.6
30 – 40	2.8674	0.7	2.8600	0.8	2.8663	0.7	2.8651	0.4
40 – 50	2.9550	0.7	2.9451	0.9	2.9183	0.7	2.9390	0.4
50 – 60	2.9766	0.7	2.9283	0.9	2.9729	0.7	2.9634	0.4
60 – 80	2.9439	0.6	2.9529	0.7	2.9365	0.6	2.9435	0.4
80 – 100	3.0052	0.6	3.0059	0.7	3.0104	0.6	3.0071	0.4
100 – 120	2.9720	0.6	2.9933	0.7	2.9582	0.7	2.9738	0.4
120 – 150	–	–	3.0312	0.6	–	–	3.0312	0.6
150 – 175	–	–	3.0373	0.7	–	–	3.0373	0.7
175 – 200	–	–	2.9686	0.8	–	–	2.9686	0.8
200 – 225	–	–	2.9070	1.1	–	–	2.9070	1.1
30 – 80	2.9357	0.4	2.9216	0.4	2.9235	0.4	2.9278	0.2

Table 14: FINAL NEUTRON CAPTURE CROSS SECTION RATIOS OF ^{175}Lu AND ^{176}Lu RELATIVE TO ^{197}Au

Energy Bin[a] (keV)	$\frac{\sigma(^{175}Lu)}{\sigma(^{197}Au)}$	Uncertainty (%)			$\frac{\sigma(^{176}Lu)}{\sigma(^{197}Au)}$	Uncertainty (%)		
		stat	sys	tot		stat	sys	tot
3 – 5	1.8569	4.3	0.7	4.4	2.4463	3.9	0.8	4.0
5 – 7.5	1.7513	2.6	0.7	2.7	2.4264	2.3	0.8	2.4
7.5 – 10	2.0354	2.1	0.7	2.2	2.8057	1.9	0.8	2.1
10 – 12.5	1.8575	1.6	0.7	1.7	2.5093	1.4	0.8	1.6
12.5 – 15	2.0356	1.4	0.7	1.6	2.7729	1.3	0.8	1.5
15 – 20	2.1478	0.9	0.7	1.1	2.8571	0.8	0.8	1.1
20 – 25	2.2732	0.8	0.7	1.1	3.0611	0.7	0.8	1.1
25 – 30	2.1538	0.6	0.7	0.9	2.9176	0.6	0.8	1.0
30 – 40	2.1558	0.5	0.7	0.9	2.8651	0.4	0.8	0.9
40 – 50	2.2551	0.5	0.7	0.9	2.9390	0.4	0.8	0.9
50 – 60	2.2234	0.5	0.7	0.9	2.9634	0.4	0.8	0.9
60 – 80	2.2101	0.4	0.7	0.8	2.9435	0.4	0.8	0.9
80 – 100	2.2728	0.4	0.7	0.8	3.0071	0.4	0.8	0.9
100 – 120	2.1917	0.4	0.7	0.8	2.9738	0.4	0.8	0.9
120 – 150	2.0394	0.8	0.7	1.1	3.0312	0.6	0.8	1.0
150 – 175	1.9435	0.8	0.7	1.1	3.0373	0.7	0.8	1.1
175 – 200	1.8961	0.9	0.7	1.1	2.9686	0.8	0.8	1.1
200 – 225	1.8699	1.3	0.7	1.5	2.9070	1.1	0.8	1.4

[a] Energy bins as used for calculating the Maxwellian averaged cross sections

5 DISCUSSION OF UNCERTAINTIES

The determination of statistical and systematic uncertainties followed the procedures applied in previous measurements with the 4π BaF_2 detector [16, 17]. Therefore, a discussion of the particular aspects of the present experiment may suffice here. The various contributions to the overall uncertainties are compiled in Table 16.

The binding energy for both lutetium isotopes is sufficiently low that the scattering background could be normalized in the sum energy region around 9 MeV. Therefore, no systematic differences were observed in the data, neither between individual runs nor correlated with the different acquisition modes or evaluation methods (see Tables 12 and 13). Accordingly, systematic uncertainties in background subtraction were negligible as in the measurements on the samarium [16], gadolinium [21], and dysprosium [24] isotopes.

The minor systematic uncertainties related to the flight path measurement and the neutron flux normalization have been discussed previously.

Table 15: NEUTRON CAPTURE CROSS SECTIONS OF ^{175}Lu, AND ^{176}Lu (in mb).

Energy Bin (keV)	$\sigma(^{197}\mathrm{Au})^a$	$\sigma(^{175}\mathrm{Lu})$	$\sigma(^{176}\mathrm{Lu})$
3 – 5	2266.7	4209.	5545.
5 – 7.5	1726.7	3024.	4190.
7.5 – 10	1215.7	2475.	3411.
10 – 12.5	1066.7	1981.	2677.
12.5 – 15	878.0	1787.	2435.
15 – 20	738.8	1587	2111.
20 – 25	600.0	1364.	1837.
25 – 30	570.8	1230.	1665.
30 – 40	500.4	1079.	1434.
40 – 50	433.3	977.2	1274.
50 – 60	389.6	866.3	1155.
60 – 80	349.4	772.1	1028.
80 – 100	298.3	678.0	897.0
100 – 120	290.1	635.9	862.8
120 – 150	274.1	559.1	830.9
150 – 175	263.7	512.4	800.8
175 – 200	252.6	478.9	749.8
200 – 225	248.5	464.6	722.3

[a]Based on the ^{197}Au data discussed in text

The enriched samples contained several impurities at the level of about 50 ppm, but the total contamination was less than 0.06% in both cases. For the natural sample this contamination was below 6 ppm. The rare earth contamination consisted only of ytterbium, which contributed less than 0.2% to the enriched and 50 ppm to the natural sample. Since the capture cross sections of the impurities were smaller than or compatible with those of the Lu isotopes, a systematic uncertainty of 0.2% was sufficient to account for the impurities.

The isotopic composition was specified with absolute uncertainties between 0.1% and 0.2% (Table 2). Though these seem to be rather conservative numbers [30] they were adopted in data analysis, resulting in relative uncertainties of 0.2% and 0.3% for the mass of the main isotopes in the ^{175}Lu and ^{176}Lu sample, respectively.

The uncertainty related to the isotopic correction has been discussed in detail elsewhere [24, 21]. For the rather large correction required for the ^{176}Lu sample, this uncertainty can be evaluated from the spectra in Fig. 4. In the evaluated energy range from threshold up to 7.7 MeV, the count rate in the upper spectrum consists of contributions from captures in ^{176}Lu (76.5%), in ^{175}Lu (21.8%), and from capture from scattered neutrons (1.7%). If the absolute uncertainty of 0.2% for the main isotope and for the ^{175}Lu is taken into account, the impurity correction implies an uncertainty of 0.4%. For the ^{175}Lu and the natural lutetium samples, the small isotopic corrections give an uncertainty of 0.2% at most.

Samples with low enrichment are also problematic with respect to the correction for

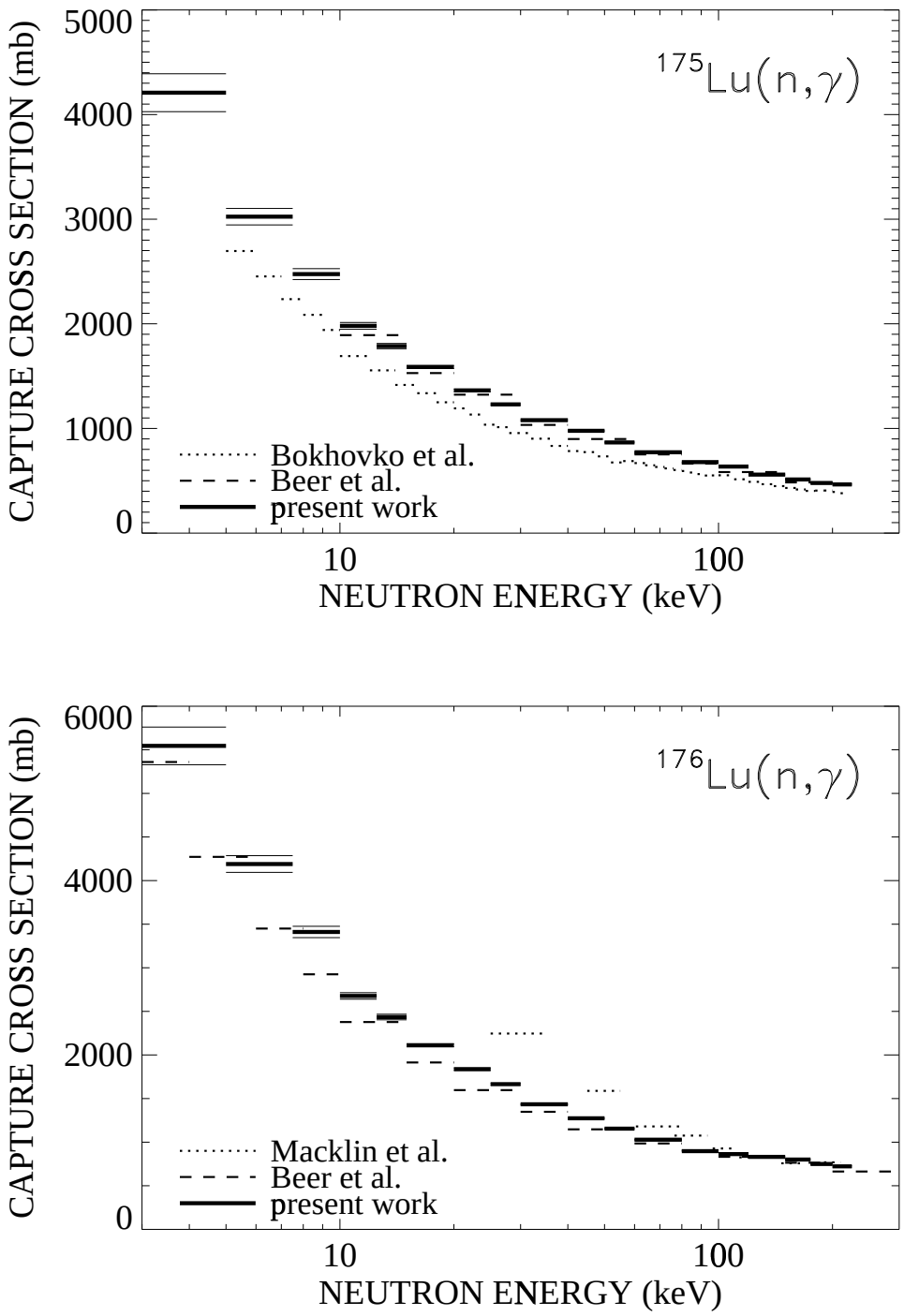

Figure 9: The neutron capture cross sections of ^{175}Lu and ^{176}Lu compared to the data of Beer *et al.* , Bokhovko *et al.* , and Macklin *et al.* [11, 12, 14].

Table 16: SYSTEMATIC UNCERTAINTIES (%)

Flight path	0.1
Neutron flux normalization	0.2
Sample mass: elemental impurities	0.2
Isotopic composition (^{175}Lu/ ^{176}Hf)	0.2/0.3
Isotopic correction (^{175}Lu/ ^{176}Lu)	0.2/0.4
Multiple scattering and self–shielding: F_2 cross section ratio	0.4
Undetected events: F_1 cross section ratio	0.4
total systematic uncertainties	
$\sigma(^{175}\mathrm{Lu})/\sigma(\mathrm{Au})$	0.7
$\sigma(^{176}\mathrm{Lu})/\sigma(\mathrm{Au})$	0.8

multiple scattering and self-shielding. Subtraction of the normalized spectra of the impurity isotopes may either be insufficient or may even overcompensate the multiple scattering effect. This holds certainly if the individual sample masses are significantly different as in case of ^{176}Lu. For the ^{176}Lu sample the effect was not visible in the spectra but may still cause a small uncertainty. Therefore, the calculation of the correction factors MS was performed twice, before and after the correction for isotopic impurities. The respective difference is 1.0% for the ^{176}Lu sample, nearly independent of neutron energy. In anology to the gadolinium and dysprosium experiments [21, 24], 25% of this difference were adopted as the related additional uncertainty and were added to the uncertainty provided by the SESH code [19]. For the ^{175}Lu sample this effect is negligible due to the high enrichment.

The detailed discussion of the systematic uncertainties due to undetected events for the gadolinium experiment [21] showed that uncertainties of the correction factor F_1 were 0.3% for the even and 0.8% for the odd isotopes. These corrections were based on two independent sets of calculated capture cascades, and were found to agree with the respective uncertainties quoted in previous measurements with the 4π BaF_2 detector [16, 17, 27]. It turned out that this uncertainty was mainly determined by the difference in binding energy between the investigated isotope and the gold standard, which is large for the odd, but small for the even gadolinium isotopes. This result was verified by using experimental γ-ray cascades from capture on various dysprosium isotopes [24], thus confirming the reliability of the evaluated uncertainties. With this procedure, an uncertainty of 0.4% was assigned for the two lutetium isotopes.

6 MAXWELLIAN AVERAGED CROSS SECTIONS

Maxwellian averaged cross sections were calculated in the same way as described in Refs. [17, 23]. The neutron energy range from 0 - 700 keV was divided into three intervals I_x according to the origin of the adopted cross sections (see Table 17). The dominant part I_2 between 3 and 225 keV is provided by the present experiment (Table 15). These data were obtained with sufficient resolution in neutron energy to exclude systematic uncertainties that may result in the calculation of the Maxwellian average if the energy grid is too coarse.

The contribution I_1 was determined by normalizing the cross sections of Kopecky *et al.* [31] to the present data in the interval between 3 and 10 keV. Since the shape of both data sets were found in good agreement, an uncertainty of 5% was assumed for the contribution I_1.

At typical *s*-process temperatures the energy interval from 225 to 700 keV contributes very little to the Maxwellian average. For this part, the data of Kopecky *et al.* [31] were normalized to the present results between 50 and 225 keV, and the corresponding uncertainties were assumed to increase from 2% at 225 keV to 10% at 700 keV.

The systematic uncertainties of the Maxwellian averaged cross sections in Table 17 are determined by the uncertainties of the measured cross section ratios in the interval I_2 (Table 14) as well as by the respective I_1 and I_3 contributions. The 1.5% uncertainty of the gold standard was not included since it cancels out in most applications of relevance for *s*-process studies. In general, the systematic uncertainties dominate over the statistical uncertainties, except at low thermal energies.

The present results at kT=30 keV are eventually compared in Table 18 with previous experiments and with the compilations of Bao *et al.* [6] and Beer, Voss, and Winters [32]. For ^{175}Lu good agreement is found to the four older measurements. In fact, the present value agrees to better than 1% with the average of these four data sets, whereas the more recent value based on the measurement of Bokhovko *et al.* is significantly smaller. For ^{176}Lu the present result is systematically larger than the TOF measurements by Beer *et al.* , which were performed at different accelerators, while it is in agreement with their older activation. This feature may reflect problems with the large correction for isotopic impurities that affects only the TOF measurement. Accordingly, the present data are systematically larger by $\sim$7% compared to recent evaluations [6, 32] and exhibit five times smaller uncertainties.

Table 17: MAXWELLIAN AVERAGED NEUTRON CAPTURE CROSS SECTIONS OF THE LUTETIUM ISOTOPES.

^{175}Lu							
ΔE	0 - 3 keV	3 - 225 keV	225 - 700 keV	Thermal Spectrum			
Data:	from Ref. [31][a]	this work	from Ref. [31][a]				
kT	I_1	I_2	I_3	$<\sigma v>/v_T$ (mbarn)			
(keV)	(mbarn)	(mbarn)	(mbarn)		stat	sys[b]	tot
8	508.1±25.	2153.±21.	0.0	2661.	33.	19.	38.
10	338.6±17.	1970.±16.	0.0	2309.	23.	16.	28.
15	158.9±7.9	1643.±9.7	0.0	1802.	13.	13.	18.
20	91.9±4.6	1433.±6.9	0.1	1525.	8.3	11.	14.
25	59.8±3.0	1286.±5.4	0.4	1346.	6.2	9.4	11.
30	42.0±2.1	1175.±4.5	1.5	1219.	5.0	8.5	9.9
40	23.9±1.2	1012.±3.5	7.5±0.2	1043.	3.7	7.3	8.2
50	15.5±0.8	889.9±2.9	18.5±0.5	923.9	3.0	6.5	7.2
52	14.3±0.7	868.5±2.8	21.2±0.6	904.0	2.9	6.3	6.9
60	10.8±0.5	790.2±2.6	32.6±1.0	833.6	2.8	5.8	6.4
70	8.0±0.4	705.4±2.3	47.6±1.5	761.0	2.8	5.3	6.0
80	6.1±0.3	632.4±2.1	62.0±2.1	700.5	3.0	4.9	5.7
90	4.8±0.2	569.0±1.9	75.1±2.7	648.9	3.3	4.5	5.6
100	3.9±0.2	513.8±1.8	86.3±3.2	604.0	3.7	4.2	5.6
^{176}Lu							
ΔE	0 - 3 keV	3 - 225 keV	225 - 700 keV	Thermal Spectrum			
Data:	from Ref. [31][a]	this work	from Ref. [31][a]				
kT	I_1	I_2	I_3	$<\sigma v>/v_T$ (mbarn)			
(keV)	(mbarn)	(mbarn)	(mbarn)		stat	sys[b]	tot
8	674.7±34.	2911.±25.	0.0	3586.	42.	29.	51.
10	449.8±22.	2659.±19.	0.0	3109.	29.	25.	38.
15	211.2±11.	2210.±12.	0.0	2421.	16.	19.	25.
20	122.1±6.1	1924.±8.2	0.1	2046.	10.	16.	19.
25	79.5±4.0	1726.±6.4	0.6	1806.	7.5	14.	16.
30	55.8±2.8	1581.±5.3	2.3±0.1	1639.	6.0	13.	14.
40	31.8±1.6	1371.±4.1	11.1±0.3	1414.	4.4	11.	12.
50	20.6±1.0	1216.±3.5	27.2±0.8	1264.	3.7	10.	11.
52	19.0±1.0	1189.±3.4	31.1±0.9	1239.	3.7	9.9	11.
60	14.4±0.7	1088.±3.1	47.9±1.5	1150.	3.5	9.2	9.8
70	10.6±0.5	978.3±2.8	69.9±2.3	1059.	3.7	8.5	9.3
80	8.1±0.4	882.0±2.6	91.2±3.1	981.3	4.1	7.8	8.8
90	6.4±0.3	797.3±2.4	110.3±3.9	914.0	4.6	7.3	8.6
100	5.2±0.3	722.8±2.2	126.8±4.6	854.8	5.1	6.8	8.5

Table 18: MAXWELLIAN AVERAGED CROSS SECTIONS AT kT=30 keV COMPARED TO PREVIOUS EXPERIMENTS AND EVALUATIONS

Isotope	Experiment		Evaluation	
	Cross section (mb)	Reference	Bao *et al.* [6]	Beer, Voss, Winters [32]
^{175}Lu	1219 ± 10	present work[a]	1146±44	1179±44
	992 ± 50	Bokovko *et al.* (92) [12]		
	1179 ± 44	Beer *et al.* (84) [11]		
	1266 ± 43	Beer *et al.* (81) [7]		
	1206 ± 54	Macklin *et al.* (78) [33]		
	1265 ± 190	Lepine *et al.* (72) [34]		
^{176}Lu	1639 ± 14.	present work[a]	1532±69	1537±60
	1526 ± 69	Beer *et al.* (84) [11]		
	1514 ± 56	Beer *et al.* (84) [11]		
	1718 ± 85	Beer *et al.* (80) [15]		
	2236 ± 335	Sorin *et al.* (73) [13]		

[a] The 1.5% uncertainty of the gold cross section is not included, since it cancels out in most applications of relevance for nuclear astrophysics.

7 ACKNOWLEDGEMENTS

We are indebted to G. Rupp for his invaluable technical assistance which was essential for the success of this work. The hospitality of Forschungszentrum Karlsruhe is gratefully acknowledged by L.K.

References

[1] F. Käppeler, G. Schatz, and K. Wisshak, Report KfK-3472, Kernforschungszentrum Karlsruhe, Karlsruhe Germany, 1982.

[2] E. Anders and N. Grevesse, Geochim. Cosmochim. Acta **53**, 197 (1989).

[3] J. Best, H. Stoll, C. Arlandini, S. Jaag, F. Käppeler, K. Wisshak, A. Mengoni, G. Reffo, and T Rauscher, Phys. Rev. C **64**, 015801 (2001).

[4] F. Käppeler, K.A. Toukan, M. Schumann, and A. Mengoni, Phys. Rev. C **53**, 1397 (1996).

[5] S. O'Brien, S. Dababneh, M. Heil, F. Käppeler, R. Plag, R. Reifarth, R. Gallino, and M. Pignatari, Phys. Rev. C **68**, 035801 (2003).

[6] Z.Y. Bao, H. Beer, F. Käppeler, F. Voss, K. Wisshak, and T. Rauscher, Atomic Data Nucl. Data Tables **76**, 70 (2000).

[7] H. Beer, F. Käppeler, K. Wisshak, and R. Ward, Astrophys. J. Suppl. Series **46**, 295 (1981).

[8] N. Klay, F. Käppeler, H. Beer, and G. Schatz, Phys. Rev. C **44**, 2839 (1991).

[9] C. Doll, H.G. Börner, S. Jaag, F. Käppeler, and W. Andrejtscheff, Phys. Rev. C **59**, 492 (1999).

[10] K. Wisshak, F. Voss, F. Käppeler, and M. Krtička, Report FZKA6962, Forschungszentrum Karlsruhe, Karlsruhe Germany 2004.

[11] H. Beer, G. Walter, R.L. Macklin, and P.J. Patchett, Phys. Rev. C **30**, 464 (1984).

[12] M.V. Bokhovko, V.N. Kononov, E.D. Poletaev, N.S. Rabotnov, and V.M. Timokhov, in *Nuclear Data for Science and Technology*, edited by S. Qaim (Springer, Berlin, 1992), p. 62.

[13] V.S. Shorin, V.M. Gribunin, V.N. Kononov, and I.I. Sidorova, Astrophys. J. **7**, 286 (1973).

[14] R.L. Macklin and J.H. Gibbons, Phys. Rev. **159**, 1007 (1967).

[15] H. Beer and F. Käppeler, Phys. Rev. C **21**, 534 (1980).

[16] K. Wisshak, K. Guber, F. Voss, F. Käppeler, and G. Reffo, Phys. Rev. C **48**, 1401 (1993).

[17] K. Wisshak, F. Voss, F. Käppeler, and G. Reffo, Phys. Rev. C **45**, 2470 (1992).

[18] K. Wisshak, K. Guber, F. Käppeler, J. Krisch, H. Müller, G. Rupp, and F. Voss, Nucl. Instr. Meth. A **292**, 595 (1990).

[19] F. H. Fröhner, Technical report, GA-8380, Gulf General Atomic (1968).

[20] C. Nordborg, H. Gruppelaar, and M. Salvatores, in *Nuclear Data for Science and Technology*, edited by S. Qaim (Springer, Berlin, 1992), p. 782.

[21] K. Wisshak, F. Voss, F. Käppeler, K. Guber, L. Kazakov, N. Kornilov, M. Uhl, and G. Reffo, Phys. Rev. C. **52**, 2762 (1995).

[22] K. Wisshak, F. Voss, F. Käppeler, L. Kazakov, and G. Reffo, Report FZKA5967, Forschungszentrum Karlsruhe, Karlsruhe, Germany 1997.

[23] K. Wisshak, F. Voss, F. Käppeler, and G. Reffo, Phys. Rev. C. **42**, 1731 (1990).

[24] F. Voss, K. Wisshak, C. Arlandini,K. Käppeler, L. Kazakov, and T. Rauscher, Phys. Rev. C **59**, 1154 (1999).

[25] A. Gilbert and A.G.W. Cameron, Can. J. Phys. **43**, 1446 (1965).

[26] J. F. Mughabghab, M. Divadeenam, and N. E. Holden, in *Neutron Cross Sections, Vol. 1, Part A* (Academic Press, New York, 1981).

[27] F. Voss, K. Wisshak, K. Guber, F.Käppeler, and G. Reffo, Phys. Rev. C **50**, 2582 (1994).

[28] R. L. Macklin, private communication (unpublished).

[29] W. Ratynski and F. Käppeler, Phys. Rev. C **37**, 595 (1988).

[30] K. Wisshak, F. Voss, F. Käppeler, L. Kazakov, and G. Reffo, Phys. Rev. C. **57**, 391 (1998).

[31] J. Kopecky, J.-Ch. Sublet, J.A. Simpson, R.A. Forrest, and D. Nierop, Report INDC(NDS)-362, International Atomic Energy Agency, Vienna, Austria, 1997.

[32] H. Beer, F. Voss, and R.R. Winters, Astrophys. J. Suppl. **80**, 403 (1992).

[33] R.L. Macklin, D. Drake, and J. Malanify, Technical report LA-7479-MS, Los Alamos National Laboratory (1978).

[34] J. Lepine, R. Douglas, and H. Maia, Nucl. Phys. A **196**, 83 (1972).